Molecular structure and linear-non linear rheology relation of rice starch during milky, dough, and mature stages

Ranathunga, Ashoka; Suwannaporn, Prisana; Kiatponglarp, Worawikunya; Wansuksri, Rungtiva; Sagis, Leonard M.C.

Molecular structure and linear-non linear rheology relation of rice starch during milky, dough, and mature stages

Ashoka Ranathunga [a], Prisana Suwannaporn [a,*], Worawikunya Kiatponglarp [b], Rungtiva Wansuksri [c], Leonard M.C. Sagis [d]

[a] *Department of Food Science & Technology, Kasetsart University, Chatuchak, Bangkok 10900, Thailand*
[b] *Synchrotron Light Research Institute, Muang District, Nakhon Ratchasima 30000, Thailand*
[c] *Cassava and Starch Technology Research Team, National Center for Genetic Engineering and Biotechnology, National Science and Technology Development Agency, Pathum Thani 12120, Thailand*
[d] *Physics and Physical Chemistry of Food, Department of Agrotechnology and Food Sciences, Wageningen University, Bornse Weilanden 9, 6708 WG Wageningen, The Netherlands*

A R T I C L E   I N F O

A B S T R A C T

Immature rice has potential to be used as healthy food. The relation between molecular structure and rheological properties was investigated. The lamellar repeating distance (8.42–8.63 nm) and crystalline thickness (4.60–4.72 nm) were not different among stages indicating a complete lamellar structure even at early stage. The relative crystallinity was higher in dough (39.62 %) than milky (36.69 %) and mature starch (35.22 %) caused by molecular structure, amylose, and amylose-lipid complex. The short amylopectin branched chains (A and B1) in dough starch were easily entangled resulted in higher Payne effect and elastic dominant. Dough starch paste exhibited higher G'_{Max} (738 Pa) than milky (685 Pa) and mature (645 Pa) starch. In a non-linear viscoelastic regime, small strain hardening was found in milky and dough starch. Mature starch showed the highest plasticity and shear thinning at high-shear strains as the long-branched chains (B3) microstructure was disrupted, disentangled, followed by chain orientation along shear.

1. Introduction

Immature grain from wheat, rye, and rice has been consumed as a nourishing food for thousands of years in the Middle East, North-African, and Southeast-Asian countries. In Thailand, immature rice is used in traditional foods such as young rice milk and green rice flake. Immature rice has been reported to have high nutritional value, is easy to digest, and has low allergenicity with potential to be used as a new source of healthy foods (Pantoa et al., 2020; Ranathunga & Suwannaporn, 2022). The molecular structures of rice starch in relation to functional properties particularly rheological properties are important for food applications. However, most studies on structure-functional properties relation have been done on mature starch.

Amylose and amylopectin are the two major glucan polymers that radially arrange to form semi-crystalline structure in starch granules. Starch synthase, branching enzyme, and debranching enzyme are the main enzymes evolved with starch biosynthesis. The granule-bound starch synthases responsible for amylose synthesis, while starch

synthases evolved with the elongation of glucan and branched glucan or amylopectin production. Starch synthases produce branched glucan while branching and debranching enzymes play roles in forming a semi-crystalline structure of starch granule (Li et al., 2021). The rate of change of these enzymes' activities influence the production of starch with different proportions of amylose and amylopectin. The amylopectin chain length (CL) distribution, especially long chain amylopectin, was reported to have a strong effect on rheological and physicochemical properties of mature rice starch. Starch that contained longer average branch CL of amylopectin, generated shear resistant, firm, and stronger gels with higher retrogradation by making higher intermolecular bonds amylose molecules (Jane & Chen, 1992). The long chain amylopectin fraction (DP > 67) in cassava starch was reported to entangle with amylose chains, causing a strong and firm gel with high shear resistance and moduli with low frequency dependence. Starch with long chain amylopectin was important for gel production with better shear resistance and higher firmness (Jane & Chen, 1992). The long chain amylopectin in mature rice starch was positively correlated with paste

---

* Corresponding author.
E-mail address: prisana.s@ku.ac.th (P. Suwannaporn).

viscosity and breakdown viscosity due to higher hydration capacity and intermolecular interaction (Han & Hamaker, 2001; Lu et al., 1997). Texture of rice starch was controlled by the proportion of long (DP 92–98) and short chain (DP ≤ 25) amylopectin (Ong & Blanshard, 1995). In waxy rice starch, the long chain amylopectin contributed to the development of a gel network. The long-chain fraction was negatively correlated with loss tangent (tan δ) and positively correlated with the initial temperature of storage modulus increment ($T_{G'}$). The short and short to long chain ratio of amylopectin showed a positive correlation with the maximum G′ (G'_{max}) (Singh et al., 2012). The short chain amylopectin (DP 6–12) of rice starch was negatively correlated with gelatinization temperature (Kong et al., 2015). The paste viscosity and loss modulus (G″) of corn starch were positively linked to the short chain amylose and short branch chain of amylopectin (DP 6-12) (Korus et al., 2008).

In this study, the molecular structure and granular characteristics of rice starch during grain maturation including size distribution, molecular order, degree of crystallinity, amylopectin fine structure, and amylose / amylopectin ratio were investigated in relation to their rheological properties in the linear (LVE) and non-linear viscoelastic (NLVE) regime. The NLVE regime which evaluates starch at higher strain using large amplitude oscillatory shear (LAOS) is a better representation of real industrial conditions during processing. The behaviour of starch paste in the NLVE regime has been reported to be more accurate to characterize the flow patterns of starch chains under shear (Liu et al., 2021). The long amylopectin branch chains which increased with grain maturation were hypothesized to be arranged in the shear direction, with more double helical disentanglement at large deformation. However, few studies have investigated rheological properties of starch using this technique. An understanding of the relationship between structure and rheological properties of mature and immature rice starch could benefit future application of immature rice starch as a new source of health foods.

2. Materials and methods

2.1. Rice sample

Rough rice grain (KDML105 variety or Jasmine rice) was harvested during November 2020 at Watcharawan Green Farm, Payao, Thailand (25.4–17.5 °C average day-night temperature, and 61 mm precipitation). Rough rice grain at various development stages was harvested according to their physiological changes. The first days after flowering (DAF) was counted when 80 % of the rice in the field was flowering. Paddy rice at milky (15 DAF; liquid phase), dough (21 DAF; dough phase), and mature stage (28 DAF; solid phase). All rough rice grains were put in sealed plastic bags and frozen at −20 °C. Starch was then immediately extracted to avoid amylolytic activity.

2.2. Starch extraction

Rough rice grains were de-husked manually and the kernels were steeped in 0.1 % NaOH (1:20 ratio) for 16 h and drained off. Soaked rice kernels were ground with 0.1 % NaOH and filtered through a 38 μm sieve to remove bran. The resultant solution was centrifuged (4000 rpm, 10 min), and the top yellowish protein layer was scraped off. The precipitate was dispersed again with NaOH for 3 h and centrifuged until no yellowish layer was observed. The precipitate was washed several times with DI water until it reached pH 7, and dried at 50 °C until 10–12 % moisture content (mc) was obtained. The dried starch was ground and sieved through a 150 μm sieve and stored in a desiccator until further analysis.

2.3. Amylose content

Starch (100 mg) was mixed with 95 % ethanol (1 mL), 1 M NaOH (9

mL), and filled up to a volume of 100 mL using DI water. The starch solution (0.5 mL) was mixed with DI water (9.2 mL), 0.9 N NH₄Cl (0.1 mL), and 0.15 % I₂ solution (I₂ in 1.5 % KI) (0.2 mL) for 30 min. The absorbance of the solution was measured by a spectrophotometer (Metertech SP-800, Taipei, Taiwan ROC) at a wavelength of 620 nm. Amylose content was determined using a standard curve of a mixture of potato amylose (CAS 9005-82-7, Sigma Aldrich, MA, USA) and potato amylopectin (CAS: 8037-22-3, Sigma Aldrich, MA, USA) at 0, 20, 40, 60, 80 and 100 % amylose content (modified method of Pitiphunpong and Suwannaporn (2009).

2.4. Amylopectin fine structure

The rice starch (200 mg) was added with dimethylsulfoxide (DMSO) (5 mL), mixed for 8 h, and added with DI water (40 mL). The gelatinized starch solution (4.5 mL) was adjusted to pH 5.5 using 0.01 M sodium acetate buffer (0.5 mL), debranched with isoamylase (from Pseudomonas, Hayashibara Biochemical Laboratories Inc., Okayama, Japan) and pullulanase M2 (from *Bacillus licheniformis*, 1000 U/mL, Megazyme, Ireland, 10 unit). The mixture was incubated while shaking at room temperature for 12 h, and inactivated by heating for 5 min. The solution was filtered using a 0.2 μm nylon membrane and fractionated using HPAEC-PAD (DX-120, Dionex, CA, USA) with CarboPac PA100 (2 × 250 mm) column. The eluents used were a gradient of 150 mM NaOH (eluent A) and 150 mM NaOH in 500 mM sodium acetate solution (eluent B) at 0.25 mL/min flow rate. The pulsed potentials and durations were E1 = 1.05 (t1 = 400 msec), E2 = −1.05 (t2 = 10 msec) E3 = 1.55 (t3 = 10 msec) and E4 = 0.85 (t4 = 60 msec). Samples were eluted with a gradient made by increasing the proportion of eluent B; at 1–9 min from 15 to 36 %; 9–18 min from 36 to 45 %; 18–80 min from 45 to 82 %; 80–81 min from 82 to 100 %; 91–92 min from 100 to 0 % and 112–115 min from 0 to 15 % (modified method from (Bertoft, 2004).

2.5. Molecular weight of starch

The amylose and amylopectin MW was determined using a modified method of Yoo and Jane (2002). Starch (120 mg) was wetted with water (1.2 mL) and dispersed in dimethyl sulfoxide (10.8 mL). The suspension was stirred in a boiling water bath for 1 h and at room temperature for another 24 h. Starch solution (0.4 mL) was mixed with ethanol (2 mL) and the precipitated starch was centrifuged at 2300 *g* for 20 min. The precipitate was dissolved in boiling water (1.5 mL), stirred for 10 min in a boiling water bath, filtered through a nylon membrane filter (8.0 μm), and injected (2.7 mg/mL) into the high-performance size exclusion chromatography (HPSEC; Water e2695, Waters Corporation, USA) with ultra-hydrogel linear guard column (7 × 10⁶ Da) HPSEC system was equipped with a multi-angle-light-scattering detector (MALS; Dawn Heleos-II, Wyatt Tech. Corp., CA, USA), laser source (λ = 658 nm), and fused silica RI detector. The temperature of the RI detector and column were maintained at 40 °C. The mobile phase was distilled deionized water (18.2 MΩcm). Data obtained was analyzed using Astra software (Version 5.3.4, Wyatt Tech. Corp., CA, USA).

2.6. Molecular order of starch granule

2.6.1. Wide-angle X-ray scattering (WAXS)
The dry starch was placed on an aluminium window and covered with Kapton tape. The distance from the sample to the detector was 143.32 mm. The synchrotron X-ray beam (9 KeV), monochromatized by a double multilayer monochromator was applied for 300 s. The diffractograms were recorded using a LX 170 HS-CCD detector (Rayonix, IL, USA). The WAXS data was pre-processed (with background subtraction) using the SAXIST programme (Synchrotron Light Research Institute, Nakhon Ratchasima, Thailand) and visualized/normalized using Excel. The diffractogram was recorded between 3 and 30° (2θ). The graph plotting, baseline correction, and peak fitting were carried

out using Origin Pro 8 (OriginLab Corporation, MA, USA). The individual peak was fitted with Pearson VII function and the amorphous peak was fitted with Gaussian function at $2\theta = 17°$. The relative crystallinity was determined by calculating the ratio between crystalline peaks and total peaks of the diffractogram using the following equation:

$$\text{Crystallinity (\%)} = \frac{I_c}{I_a + I_c} \times 100 \tag{1}$$

Where, I_a is the amorphous area of the diffractogram, and I_c is the crystalline area of the diffractogram.

2.6.2. Small Angle X-ray Scattering (SAXS)

The dry starch was moistened to 50 % mc, placed in a thin flat aluminium window, and covered with Kapton tape. A monochromatized Synchrotron X-ray beam was applied and the SAXS profile was recorded using a SX 165-CCD detector (Rayonix LLC, IL, USA). The distance from the sample to the detector was 1776.89 mm, silver behenate ($AgC_{22}H_{43}O_2$) was used as a standard, and the exposure time was 300 s. The background and possible sources of scattering were measured using DI water and were subtracted from the SAXS pattern. The average lamellar repeat distance (α) and crystalline lamellar thickness (L) were calculated using the SAXSIT program that was developed by Synchrotron Light Research Institute using MATLAB (The MathWorks, Inc., MA, USA). The amorphous lamellar thickness (La) were calculated based on the difference between the average lamellar repeating distance (α) and the crystalline lamellar thickness (L).

2.7. Granular morphology

The granular morphology of starch was measured using a scanning electron microscope (SEM). Starch suspension (0.1 %) was uniformly mounted on a circular aluminium stub, dried at ambient temperature, and coated by sputtering with a 12 nm gold layer (Polaron Range SC7620, Quorum Technologies Ltd., Kent, UK). The images were observed at 5000× magnification under an accelerating voltage of 10 KV, using a high vacuum mode SEM (Quanta 450 FEI, Eindhoven, the Netherlands).

2.8. Starch granule size distribution

For determining the granule size distribution, starch (100 mg) was suspended in DI water (10 mL) and measured by a laser diffraction particle size analyzer (Mastersizer 2000, Malvern Instruments Ltd., Worcestershire, UK). The refractive index for water and starch was 1.33 and 1.52, respectively.

2.9. Solubility and swelling power

Starch (0.2 g) was added to DI water (10 mL), incubated in a shaking water bath at 55, 65, 75, 85, and 95 °C for 30 min, and centrifuged at 4000 rpm for 30 min. The precipitate was weighed, and the supernatant was dried at 105 °C until a constant weight was obtained. The solubility and swelling power were calculated according to Eqs. (2) and (3).

$$\text{solubility} = \frac{\text{Weight of dissolved solids in supernatant}}{\text{Weight of dry sample solids in the original sample}} \times 100 \tag{2}$$

$$\text{swelling power} = \frac{\text{Weight of sediment (w.b)}}{\text{Weight of dry sample solid} \times (100 - \text{solubility\%})} \times 100 \tag{3}$$

2.10. Steady shear flow behaviour

All rheological properties were measured using a stress-controlled rheometer (MCR302, Anton Paar, Graz, Austria). The geometry used was a cone (4°) and plate (50 mm), with a truncation gap of 0.5 mm. The

data was recorded and processed using RheoCompass 1.30 software (Anton Paar, Graz, Austria) throughout the study. Starch paste was prepared by heating a starch solution (10 %, db) at 95 °C for 30 min and cooling down to room temperature. The starch paste was transferred into the stainless-steel cone and plate geometry. Sample was equilibrated at 20 °C for 2 min before analysis. The steady shear flow behaviour of the starch paste was measured within a shear rate range of 0.1 s^{-1} to 300 s^{-1}. The data were fitted using the Herschel–Bulkley equation (Eq. (4)) (Zhang et al., 2021).

$$\sigma = \sigma_0 + k\dot{\gamma}^n \tag{4}$$

Where, σ is the shear stress (Pa), $\dot{\gamma}$ is the shear rate (s^{-1}), k is the consistency coefficient (Pa s^n), n is the flow behaviour index (dimensionless), and σ_0 is the yield stress (Pa).

2.11. Small amplitude oscillatory shear (SAOS)

For temperature sweep test, starch suspension (10 %, db) was loaded into the same geometry as above and heated using a Peltier element from 20 °C to 95 °C at a rate of 2 °C/min, kept at 95 °C for 5 min, and cooled to 20 °C using the same rate of 2 °C/min at constant frequency (1 Hz) and strain (1 %). Subsequently, a frequency sweep was conducted from 0.01 Hz to 50 Hz with constant strain (1 %). An amplitude sweep was run from 0.1 to 1000 % strain with constant frequency (1 Hz) at 20 °C. The moduli in the SAOS measurement were determined by a Fourier transform of the oscillatory stress response and calculated from the intensity and phase of the first harmonic of the spectrum within the LVE regime. The rheological properties were recorded as storage modulus (G'), loss modulus (G''), and loss tangent (G''/G'). The Payne effect (weak strain overshoot in G'') was quantified by Eq. (5).

$$H'' = \frac{G''_{max} - G''_{linear}}{G''_{linear}} \tag{5}$$

Where, G''_{linear} is the value of G'' in the LVE regime, and G''_{max} is the maximum value of G''.

2.12. Large amplitude oscillatory shear (LAOS)

The NLVE regime of rice starch paste (10 %, db) was evaluated using LAOS. The oscillation amplitude was varied in the range of 0.1 to 1000 % at constant frequency (1 Hz) at 20 °C. Lissajous plots were used to analyse the response of the starch pastes. The ratio of shear stiffening (S factor) and shear thickening (T factor) were defined using Eqs. (6) and (7), respectively (Ewoldt et al., 2008).

$$S = \frac{G'_L - G'_M}{G'_L} \tag{6}$$

$$T = \frac{\eta'_L - \eta'_M}{\eta'_L} \tag{7}$$

Where, G'_L is the shear elastic modulus at large deformation, G'_M is the shear elastic modulus at minimum strain, η'_L is the viscosity at large shear rate, and η'_M is the viscosity at minimum shear rate.

The energy dissipation per unit volume in one complete oscillatory strain cycle was evaluated by calculating the enclosed area of the Lissajous curve. The energy dissipation ratio (ϕ) was calculated by comparing the actual dissipated energy to the dissipation in a perfectly plastic deformation with the same maximum stress, as shown in Eq. (8)

$$\varnothing = \frac{\pi G''_1 \gamma_0}{4\sigma_{max}} \tag{8}$$

Where, G_1'' is the first-order viscous Fourier coefficient, σ_{max} is the maximum stress of the loop, and γ_0 is the strain amplitude.

Table 1

The mass fraction, molecular weight, and average branch chain length distribution of rice starch at various development stages.

Stage	Starch recovery (%)	*Amylose (%, db)	Average CLD (DP)	**Amylose MW			**Amylopectin MW		
				Mass[NS] fraction (%)	Mn (x10⁵)	Mw (x10⁵)	Mass fraction (%)	Mn (x10⁸)	Mw (x10⁸)
Milky	11.3 ± 0.7[c]	20.28 ± 0.19[c]	18.45 ± 0.00[a]	16.53 ± 1.76	2.05 ± 0.22	3.85 ± 0.48	83.47 ± 1.76	1.73 ± 0.43	3.19 ± 0.68
Dough	37.9 ± 2.1[b]	21.51 ± 0.10[a]	18.36 ± 0.03[b]	19.70 ± 2.92	2.18 ± 0.16	4.15 ± 0.36	80.30 ± 2.92	1.31 ± 0.15	2.83 ± 0.21
Mature	66.5 ± 3.4[a]	20.94 ± 0.19[b]	18.47 ± 0.03[a]	17.26 + 2.00	2.23 ± 0.08	4.26 ± 0.19	82.74 ± 2.00	1.29 ± 0.47	2.46 ± 1.37

[a-c]Mean ± SD with different letters in the same column indicated significant difference ($p \leq 0.05$).

*measured by colorimetric method, **measured by HPSEC.

[NS] Was not significant different ($p \leq 0.05$).
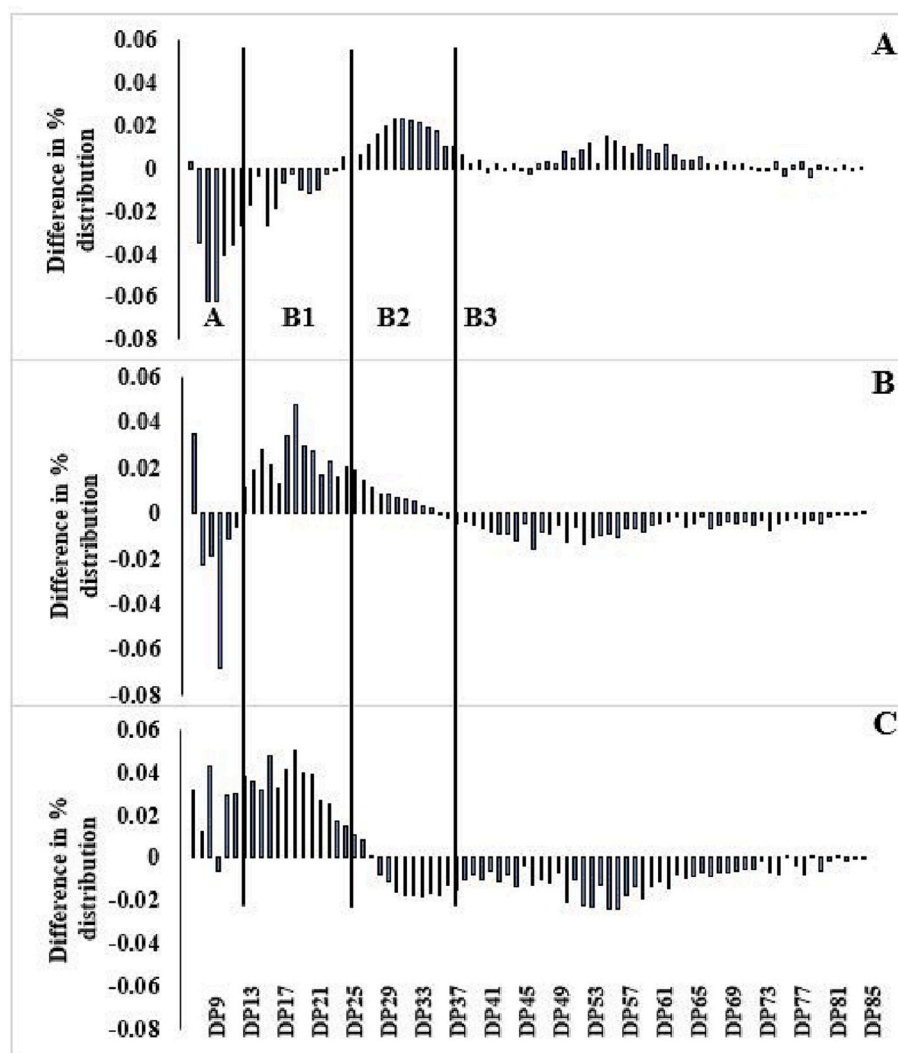
Fig. 1. The relative (%) difference of A, B1, B2, and B3 chains of (A) milky stage vs dough stage, (B) milky stage vs mature stage, and (C) dough stage vs mature stage.

2.13. Statistical analysis

All results were reported as mean and standard deviation of three replicates. Analysis of variance (ANOVA) was performed using a completely randomized design. The difference in mean was determined by Duncan's multiple range test ($p \leq 0.05$) (IBM SPSS Statistics for Windows, Version 28, IBM Corp., NY, USA).

3. Results and discussion

3.1. Amylose and amylopectin content and molecular weight

The starch recovery in mature rice grain (66.5 %) was higher than dough (37.9 %) and milky rice grain (11.3 %). Starch accumulation during maturation was reported to reach a maximum at mature stage (30 DAF) (Juliano & Tuano, 2019). The amylose content (determine by

Table 2
The WAXS relative crystallinity and SAXS lamellar structure of rice starch granules at various developing stages.

Stage	WAXs Relative crystallinity (%)	SAXs lamellar structure			
		α (nm)	Mean square deviation (σ)	L (nm)	La (nm)
Milky	36.69 ± 0.68[ab]	8.49 ± 0.06[a]	2.29	4.72 ± 0.13[a]	3.76 ± 0.03[a]
Dough	39.62 ± 1.94[a]	8.63 ± 0.16[a]	2.15	4.71 ± 0.23[a]	3.92 ± 0.07[a]
Mature	35.22 ± 0.67[b]	8.42 ± 0.03[a]	2.23	4.60 ± 0.07[a]	3.83 ± 0.01[a]

Mean + SD with different letters in the same column were significantly different ($p < 0.05$).
Note: α is the average lamellar repeating distance, L is the crystalline lamellar thickness, La is the amorphous lamellar thickness.

colorimetric method) was higher in dough starch (21.51 %) than mature (20.94 %) and milky starch (20.28 %) (Table 1). The amylose fraction determined by HPSEC was lower than colorimetric method but with the same trend. The overestimation of amylose content determined by colorimetric method was due to the interference of long chain amylopectin (Park et al., 2013). The amylose content in the early stage (5 DAF) of non-waxy Japonica rice was reported to increase from 9 % to the highest content of 18.5 % in the dough stage (17 DAF) and levelled off until fully maturation (Asaoka et al., 1985). The increase in amylose content was attributed to the differences in synthesis rate between amylose and amylopectin. The accumulation of amylose in starch granules stopped earlier than that of amylopectin, which caused the decrease in the amylose content during maturation (Asaoka et al., 1985). The gene expression of granule-bound starch synthase I (GBSSI) in rice was reported to increase until mid-stage and decrease gradually after that. The highly increase in expression levels of the gene in the middle stage (relative folds of 11.0–42.7) was higher than early stage (0.3–1.7), and last stage (1.7–7.6) of grain filling (Oko et al., 2018). The weight average MW (Mw) and number average MW (Mn) of amylose and amylopectin were not significant different among maturing stages

(Table 1). However, the MW of amylose exhibited an increasing trend towards maturity which has ever reported by Hizukuri et al. (1995). The short amylose molecules at an early stage continue to polymerize resulted in the increase of MW at mature stage. But amylopectin MW was insignificant decreased towards maturing caused by depolymerization, partly by amylolytic activity. The isoamylase and pullulanase activity were reported to be intensified in the middle and latter grain development stage (Li et al., 2009).

3.2. Molecular structure of amylopectin

The amylopectin branch CL distribution was categorized based on the degree of polymerization into different CL and included: A chain (DP 6-12), B1 (DP13-24), B2 (DP 25-36) and B3 (DP >37) (Hanashiro et al., 1996). During rice grain filling period, starch chains were cleaved by branching enzymes which were randomly transferred and linked to the original branch through the α-(1–6) linkage (Wu et al., 2013). Rice starch at all stages showed a small difference in average amylopectin CL (DP 18.36–18.47) (Table 1). A small difference in average CL of rice and waxy maize during development has been reported (Hizukuri et al., 1995; Liu et al., 2021). However, small differences in the internal chain segments and short external chains have been suggested to cause large functional differences. Waxy rice starches exhibited significant difference in gelatinization and retrogradation even though their molecular structures were quite similar (Bertoft et al., 2016).

The difference in amylopectin CL was therefore compared across stages. Results showed that the highest fraction of A and B1 chains were found in dough starch (Fig. 1). Results agreed well with Liu et al. (2021) that B1 chain firstly increased and then decreased at maturity. These short side chains easily formed double helices, which resulted in higher crystallinity and a denser amylopectin structure (Bertoft et al., 2016; Chung et al., 2011). The B1 chain, a main amylopectin branch CL, positively contributed to the number of double helices formation and a stable lamellar structure (Koroteeva et al., 2007; Zhong et al., 2021). Also in our samples, the relative crystallinity was higher in dough starch with higher A and B1 chain (Fig. 1, Table 2).

The longer B3 chain, a building block of the concentric backbone in
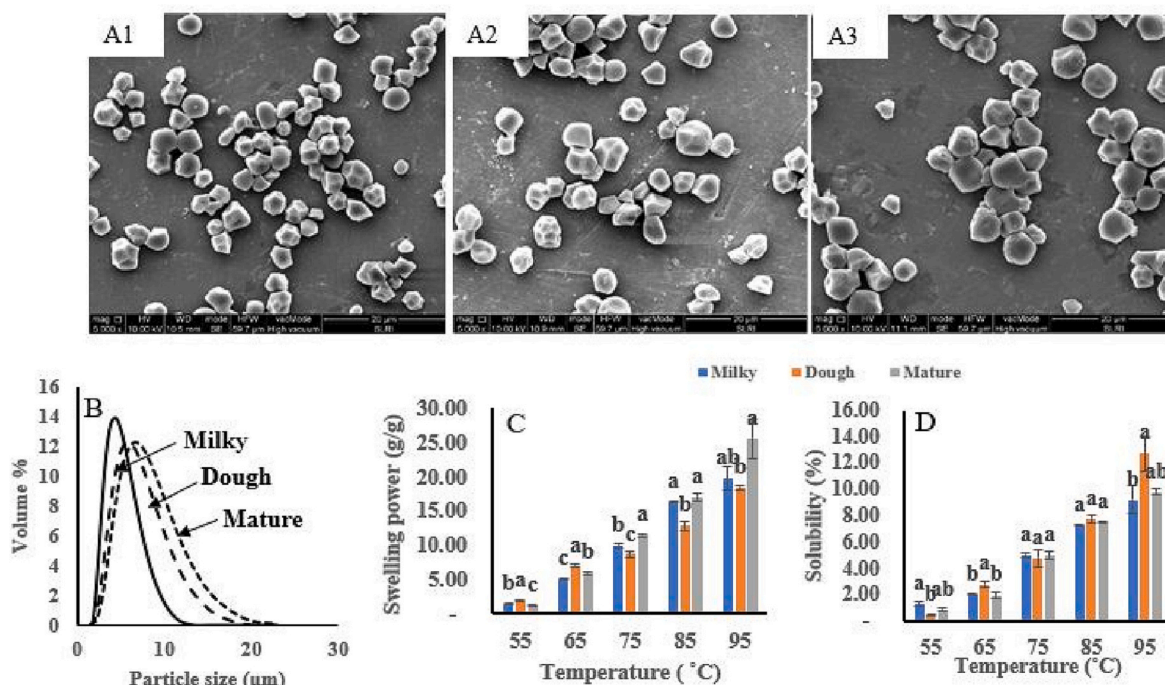
Fig. 2. SEM images of rice starch granules (5000×) of (A1) milky, (A2) dough, and (A3) mature starch (B) granule size distribution (C) swelling power and (D) solubility.
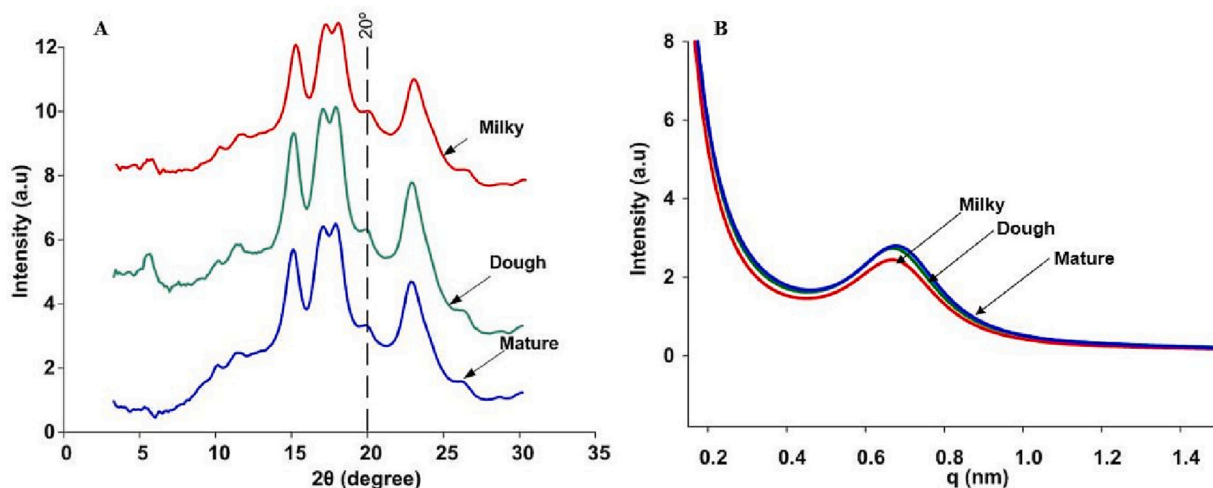
Fig. 3. The (A) WAXS and (B) SAXS patterns of rice starch granules at various developing stages. The distinct WAXs diffraction peaks at 2θ = 20° indicated amylose-lipid complex.
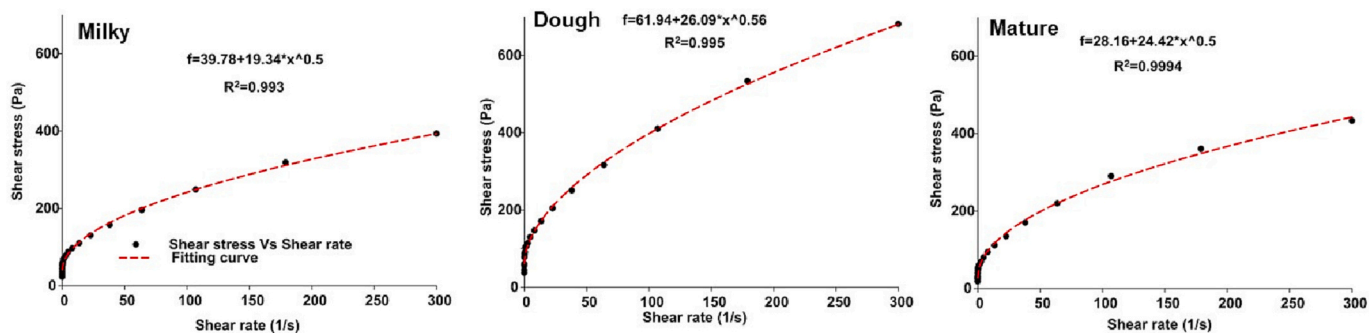
Fig. 4. Fitted flow curves as a function of shear stress vs shear rate of starch pastes at different development stages using the Herschel-Bulkley model.

Table 3

Small amplitude oscillatory shear test during heating and cooling of rice starches at various developing stages.

Stage	$T_{G'}$ (°C)	G'_{Max} (Pa)	Tan δ (at G'_{max})	$T_{G'max}$ (°C)	G'_{95} (Pa)	G'_{20} (Pa)	Tan δ (at G'_{20})
Milky	64.1 ± 0.3[a]	685 ± 34.5[a]	0.10 ± 0.0[a]	74.7 ± 1.1[a]	140 ± 8.5[a]	197 ± 5.3[b]	0.09 ± 0.0[a]
Dough	63.9 ± 0.0[a]	738 ± 36.0[a]	0.11 ± 0.0[a]	75.9 ± 0.0[a]	149 ± 5.2[a]	246 ± 7.4[a]	0.11 ± 0.0[a]
Mature	63.6 ± 0.3[a]	645 ± 19.5[a]	0.12 ± 0.0[a]	76.4 ± 0.0[a]	139 ± 2.0[a]	201 ± 18.2[b]	0.09 ± 0.0[a]

[a-b]Mean ± SD with different letters in the same column indicated significant difference ($p \leq 0.05$). $T_{G'}$ is initial temperature increment of G', G'_{Max} its maximum G', Tan δ is the loss tangent, $T_{G'max}$ is temperature at G'_{max}, G'_{95} is G' at 95°C, and G'_{20} is G' at 20 °C.

the amorphous region (Bertoft et al., 2016; Z. Li et al., 2016), was higher in mature starch (Fig. 1). Liu et al. (2021) reported the increase in B2 and B3 chains with prolonged growth period in waxy maize. These chains usually form inter-bridges with the external chains of the neighbouring molecules but cannot extend into longer double helical segments, which resulted in a lower crystallinity at mature stage (Bertoft et al., 2016).

3.3. Granular size distribution, solubility, and swelling power of starch

Starch granules in the immature stage were smaller and had a more polygonal shape, compared to the mature stage. An uneven, rough surface, and pinholes were observed in mature starch granules, which indicated endogenous enzyme activity during development (Li et al., 2007) (Fig. 2A). The volume-weighted mean diameter ($D_{4,3}$) of starch granules increased from milky (4.40 ± 0.01 μm), to dough (5.92 ± 0.01 μm), and mature stage (6.76 ± 0.01 μm) because of starch accumulation during development (Fig. 2B).

The swelling power in dough starch (18.4 g/g) was lower than milky (19.7 g/g), and mature starch (25.5 g/g) (Fig. 2C). The high amylose and amylose-lipid complex in dough starch could maintain granule integrity by limit granule hydration and swelling power. The degree of granular swelling is negatively correlated with the rigidity of starch granular structure, which is reported to be proportional to amylose content. Starch solubility at 95 °C was higher in dough (12.7 %) than in mature (9.8 %) and milky stage (9.2 %) as higher amylose caused higher amylose leaching in dough starch (Fig. 2D). Results agreed well with Chung et al. (2011) that solubility was positively correlated with amylose and leached amylose content.

3.4. Granular structure of starch granules

3.4.1. Wide angle X-ray scattering (WAXs)

The diffractogram of all starch samples exhibited similar X-ray diffraction peaks at 2θ = 15.4°, 20°, 23.1° (singlet), and 17–18° (doublet), indicating a typical A-type polymorph (Fig. 3A). The relative
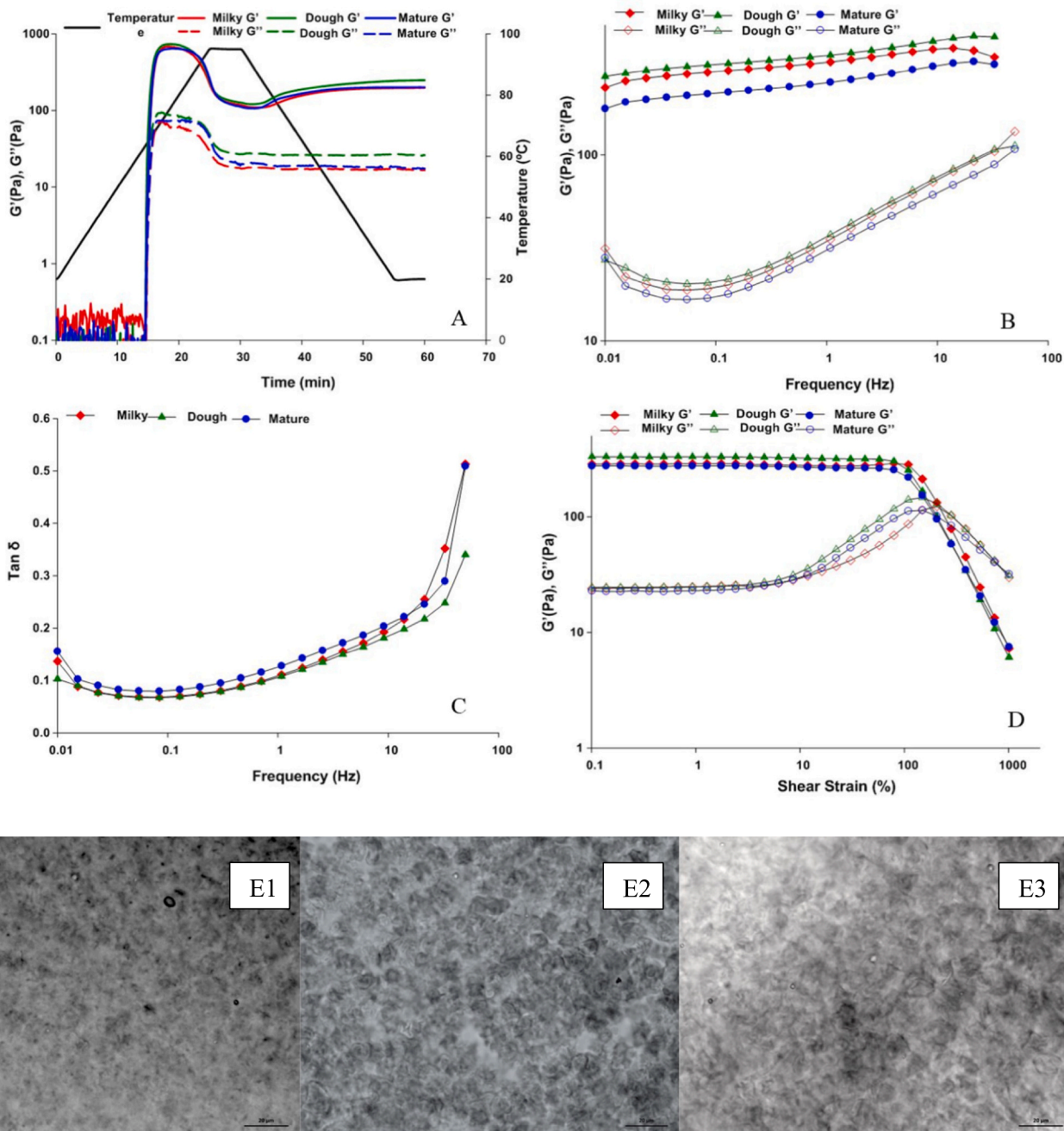
Fig. 5. Small amplitude oscillatory shear measurements (A) temperature sweep test, (B) frequency sweep test: storage and loss modulus, (C) frequency sweep test: loss tangent, (D) amplitude sweep test, (E) light microscopy image (x50) of (1) milky, (2) dough, and (3) mature starch paste.

crystallinity calculated from the area under the X-ray diffraction peaks was significant different among grain development stage. The relative crystallinity was higher in dough starch (39.62 %) than milky (36.69 %), and mature starch (35.22 %) (Table 2). The low average CL and high proportion of short A and B1 chains of dough starch resulted in a higher relative crystallinity at the dough stage. The higher short A and B1 chains developed a dense and more ordered double helices structure which increased crystallinity (Chung et al., 2011; Koroteeva et al., 2007; Zhong et al., 2021). The small difference in average CL was reported to cause a big difference in crystal type and degree of crystallinity in maize and amaranth starches (Cheetham & Tao, 1998; Kong et al., 2010). Moreover, the distinct WAXs diffraction peak was observed at $2\theta = 20°$ (Fig. 3) which indicated amylose-lipid complex of native starch (Cheetham & Tao, 1998; Li et al., 2016).

3.4.2. Small angle X-ray scattering (SAXs)

The lamellar arrangement of the semi-crystalline growth rings in starch granule formed by the side chains of amylopectin, was quantified by SAXs (Blazek & Gilbert, 2011). The SAXs pattern of all rice starches had a clear characteristic broad peak at 0.6–0.7 nm^{-1} (Fig. 3). The peak position reflects the average total thickness of the crystalline and amorphous lamellae (Zhang et al., 2023). The lamellar repeating distance (8.42–8.63 nm), mean square deviation of repeating distance (2.15–2.23 nm), and the crystalline lamellar thickness (4.60–4.72 nm), were insignificant different among development stages (Table 2). These indicated a completely molecular structural arrangement of starch granule as early as in the milky stage. The crystalline lamellar size and polymorphic structure of starches from the same botanical kind were not different (Kozlov et al., 2007). A non-significant difference in
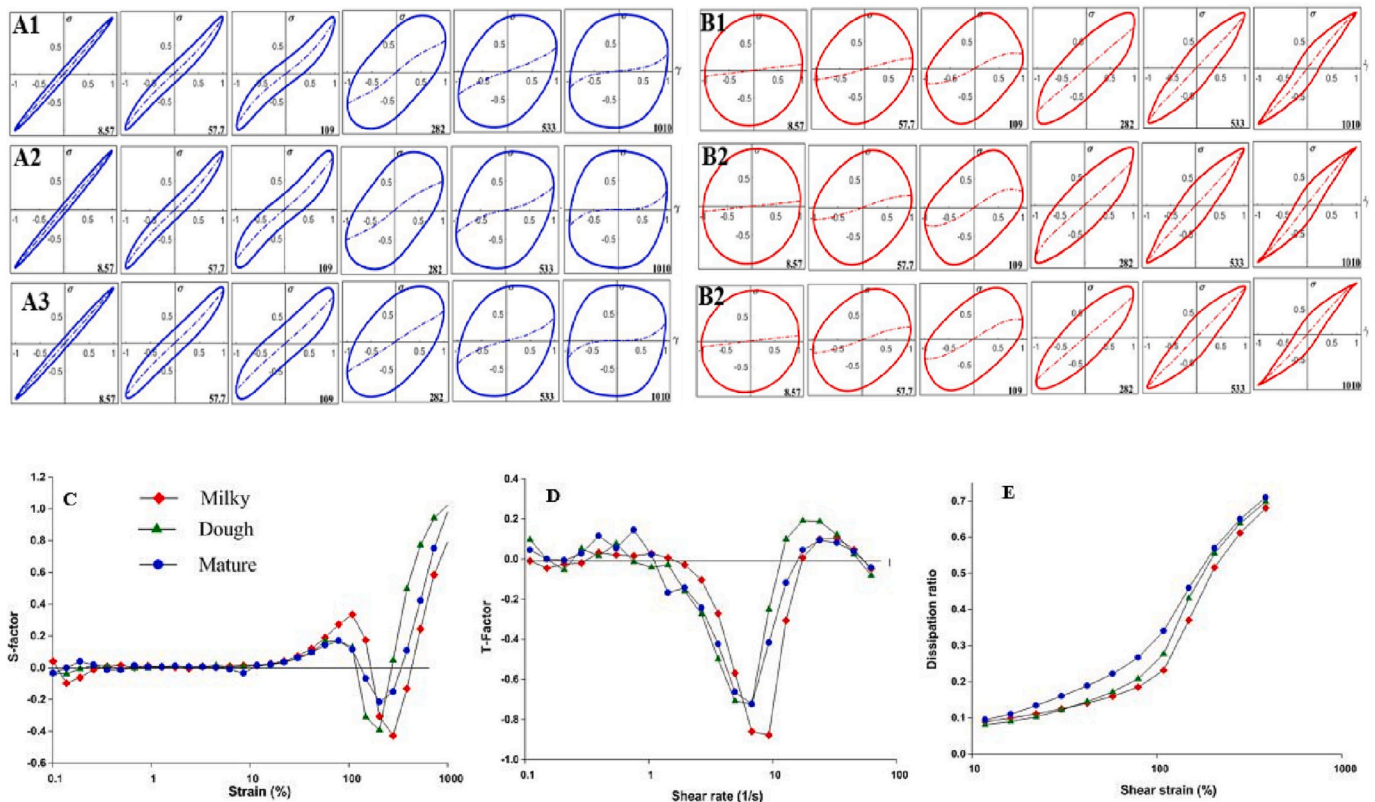
Fig. 6. Large amplitude oscillatory shear (A) normalized elastic Lissajous plots of stress-strain σ (γ), (B) normalized viscous Lissajous plots of stress-shear rate σ (γ), (C) stiffening factor, (D) thickening factor, (E) dissipation ratio of 1) milky, 2) dough, and 3) mature rice starch pastes.
Note: The applied amplitudes are listed in the right lower corner of the diagrams.

amylopectin cluster size of maize starch across the range of amylose content was also reported (Cheetham & Tao, 1998).

3.5. Steady shear rheological properties

All starch pastes showed shear-thinning behaviour in a steady shear rheometer because of the stress-induced break down of the microstructure of the starch paste. The flow curves of all rice starches could be fitted well with the Herschel-Bulkley model ($R^2 = 0.993$–0.995). All starches had flow behaviour index (n) below 1, indicated a non-Newtonian pseudoplastic behaviour (Fig. 4). The dough starch had higher consistency coefficient and yield stress (26.09 ± 3.18, 61.94 ± 3.19) than milky (19.34 ± 2.77, 39.78 ± 0.89), and mature starch (24.42 ± 1.66, 28.16 ± 1.69). The shear stress and apparent viscosity were higher in dough starch at all shear rates. The higher amylose content dough starch was more entangled, which resulted in a higher viscosity and a higher stress required to initiate flow. Starch with high amylose content was less sensitive to granular disintegration by shear forces. Moreover, the higher short A and B1 chain in dough starch, resulted in a more stable amylopectin double-helical structure and higher relative crystallinity, which better preserve granule integrity under shear. Wheat starch with shorter A and B1 chains was more elastic, whereas those with longer chains were more viscous (Zhang et al., 2020).

3.6. Small amplitude oscillatory shear (SAOS)

3.6.1. Temperature sweep test

The dough starch exhibited the highest G'_{max} and G'_{95} (738, 149 Pa, respectively) followed by milky (685, 139 Pa), and mature starch (645, 139 Pa) (Table 3, Fig. 5A). All G' of dough starch showed the highest value as it was positively correlated with amylose content, and

crystallinity. The high amylose and highly integrity starch granules indicated by more remnant starch granules in dough starch (Figure 5E2). These facilitated the formation of a strong gel network that enhance the elastic dominant properties of dough starch paste. As gel cooled down, the solubility reduced and the gel stiffness increased which was depicted as a rising G' and decayed in G''. G'_{20}, which linked to the short-term retrogradation of starch, was high in dough (246 Pa), followed by mature (201 Pa), and milky starch (196 Pa) (Table 3, Fig. 5A).

3.6.2. Frequency sweep test

All starch pastes showed an increase in G' and G'' with increased frequency (although G'' showed a slight initial decrease at frequencies below 0.1 Hz) (Fig. 5B), indicating weak gel behaviour. However, G' was higher than G'' throughout experiment indicated elastic dominant behaviour. Tan δ was lower than 1 for all frequencies, suggesting a viscoelastic gel behaviour in the applied frequency range (Fig. 5C). The higher short chains in dough starch which resulted in more double helical structure, had higher G' over the entire frequency range than mature starch (Fig. 5B). The intermolecular entanglement of leached amylose with exterior short chains of amylopectin which was high in dough starch also promoted higher G'. Starch with high amylose-lipid complex retarded granule swelling (Fig. 2C) that made it less sensitive to granular disintegration by shear force. Non-waxy rice with higher amylose content was reported to have higher G' and G'' than waxy rice (Lii et al., 1996). The G' and yield stress were positively correlated with amylose, but the loss tangent was negatively correlated with amylose content (Kong et al., 2010).

3.6.3. Amplitude sweep test

At small strains, the moduli of all rice starches were independent of the applied strain amplitude. Within the LVE regime, G' was always higher than G'', indicating a predominantly solid-like behaviour
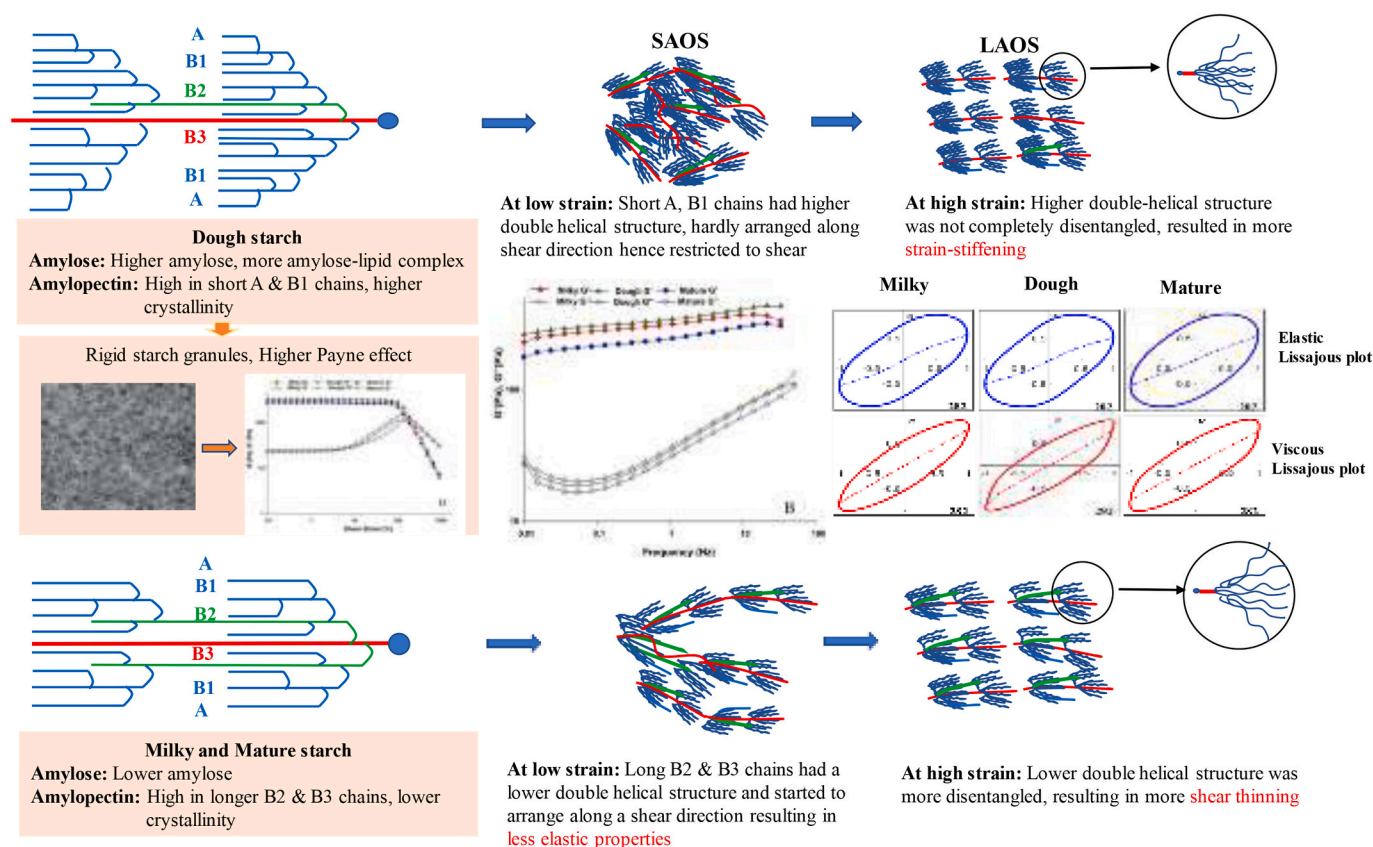
Fig. 7. Molecular starch structure and linear/non-linear rheology relation of rice starch during maturation.

(Fig. 5D). Dough starch paste had a higher G′ (3.30×10^2 Pa) than milky (2.85×10^2 Pa) and mature starch (2.74×10^2 Pa). All starch pastes showed a smooth decay in G′ when the strain amplitude was increased beyond the LVE regime reflecting strain-softening (Fig. 5D).

The curves for G″ showed a weak strain overshoot, in which the value first increased until a maximum was reached, after which it smoothly decayed. This overshoot is referred to the Payne effect, and the combined behaviour for G′ and G″ is often referred to as type III non-linear behaviour (Hyun et al., 2011). The Payne effect happened after the initial breakdown of the gel network, and its magnitude was controlled by the balance between formation and destruction of network links. In systems with dispersed particles, the effect is thought to originate from particles colliding and forming new bigger clusters, resulted in a temporary shear thickening effect (Precha-Atsawanan et al., 2018). The dough starch showed the highest magnitude of the Payne effect (H″ = 4.95), followed by milky (H″ = 3.85) and mature starch (H″ = 3.80). The higher content of granular fragments observed in dough starch could explain the higher H″ of this starch (Figure 5E2). The structure of starch paste was destroyed and reorganized to form a more stable network structure under shearing. The higher long branched chains (B3 chain) in mature starch were rearranged along the shearing direction, which weakened the entanglement among starch chains and led to a decrease in viscosity and higher shear-thinning as further disruption of the microstructure occurred (Liu et al., 2021).

3.7. Large amplitude oscillatory shear (LAOS)

3.7.1. Elastic and viscous Lissajous plots

For the smallest strain amplitude (8.57 %), the responses of all starches were still in the LVE, with a narrow ellipsoidal shape of the elastic Lissajous plot and a near circular shape of the viscous Lissajous plot. These indicated a predominantly elastic behaviour, with a

relatively small contribution of the viscous stress to the total stress (Fig. 6). At a strain amplitude of 57.7 %, weak non-linearity in the response was observed. The elastic plots became slightly wider (indicative of increased dissipation) and towards maximum intra-cycle strain. There is an increase in slope of the elastic contribution to the total stress (the dashed curve in the interior of the elastic loop), which indicated a minor degree of strain hardening in the response. The strongest effect was found in milky and dough starch, while mature starch showed no significant strain hardening at all. This strain hardening effect was not detected in the strain sweep plots using SAOS. The slight hardening effect persisted for milky and dough starch upon increasing the amplitude to 109 %, whereas the loop for mature starch was already transiting to a rhomboidal shape, indicating progressive disruption of the microstructure of this gel. Upon increasing the amplitude even further, the elastic Lissajous curves of all starches grew considerably wider, indicating an increase in plastic behaviour accounted for the amylose lipid complex formation especially in dough starch which preserved granular integrity and prevent disintegration at high shear load. (Fig. 6A). The narrow viscous Lissajous plot at high strain, with decreasing slope towards maximum intracycle shear rate, indicated shear thinning behaviour. At the highest strains, mature starch showed the highest degree of plasticity and shear thinning behaviour followed by dough and milky starch (Fig. 6B).

3.7.2. Stiffening factor, thickening factor, and dissipation ratio

The stiffening factor (S-factor) of all starches had a near zero value until a strain of 10 %, after which it started to increase to a maximum between 0.2 and 0.3 at 100 % strain (Fig. 6C). This mild strain hardening effect was observed in the intermediate strain range. At strains above 100 %, the S-factor rapidly decreased to negative values, indicating strain softening, caused by a gradual disruption of the microstructure of the gels. Milky starch showed the highest S-factor or strain stiffening,

followed by dough and mature starch. The intra-cycle stiffening observed above 400 % strain was noted as an apparent strain hardening and not a true strain hardening. At these strains, the elastic Lissajous plots had a near rectangular shape, as a result, G'_M moved towards zero. The S-factor then approached a value of 1 (see Eq. (6)). At these strains, the stress response was fully dominated by the viscous stress.

The thickening factor (T-factor) of all starch pastes were closed to zero up to a shear rate of $1\ s^{-1}$ and then became negative at higher shear rate, implying intra-cycle shear thinning behaviour (Fig. 6D). The final increase in the curve was again an artefact stemming from the definition of the T-factor and not a true thickening effect. At low shear strain, all starch pastes had a low dissipation ratio around 0.1, corresponding to a predominantly elastic behaviour. At higher shear strain, the dissipation ratio progressively increased indicating a gradual disruption of the microstructure of the gels and a transition to more viscous behaviour (Fig. 6E). The mature starch had the highest dissipation ratio over the entire strain range because of the higher proportion of long B chain that developed a weak and easily disrupted structure, as previously mentioned.

3.8. Molecular structure and linear/non-linear rheology relation

The higher short A and B1 chain altogether with higher amylose and amylose lipid complex resulted in higher crystallinity in dough starch. As a result, dough starch showed the highest G′ and Payne effect but the lowest tan δ indicating a high stiffness and a more elastic behaviour at low strain within the LVE regime using SAOS. Mature starch was high in longer B2 and B3 chain that caused lower crystallinity and was prone to disentangle arrange along the shear direction (Fig. 7).

At high strain within the NLVE regime using LAOS, the higher content of double-helical structure in dough starch was not completely disentangled, which resulted in more strain-stiffening and a stronger Payne effect (Fig. 7). However, in the high-shear rate region, the long branched chains promoted the disentanglement and chain orientation along the direction of shear which resulted in a weaker structure and a decrease in viscosity and increased shear thinning.

4. Conclusions

Dough starch had a higher fraction of amylose and small amylopectin branch chains A and B1 that easily form helices and stable lamellar structures which resulted in higher crystallinity. However, the lamellar repeat distance and crystalline thickness of all starches were insignificant different. Dough starch also exhibited the highest yield stress, apparent viscosity, G′$_{max}$, G′$_{95}$, and G′$_{20}$. In frequency sweep, dough starch had the highest value for G′ and lowest tan δ, indicated a higher stiffness than mature starch. The highest Payne effect observed in dough starch resulted from collisions of granule remnants, which increased the volume fraction of particles due to the temporary formation of larger clusters. In LAOS, the milky and dough starch paste showed higher strain hardening and S-factor, but lower dissipation ratio than mature starch. This study suggests the unique rheological properties of dough rice starch which could be used in an innovative food application with healthy aspects.

Declaration of competing interest

The authors declare that they have no known competing financial interests or personal relationships that could have appeared to influence the work reported in this paper.

Data availability

Data will be made available on request.

References

Asaoka, M., Okuno, K., Sugimoto, Y., & Fuwa, H. (1985). Developmental changes in the structure of endosperm starch of rice (Oryza sativa L.). *Agricultural and Biological Chemistry, 49*, 1973–1978.

Bertoft, E. (2004). On the nature of categories of chains in amylopectin and their connection to the super helix model. *Carbohydrate Polymers, 57*, 211–224.

Bertoft, E., Annor, G. A., Shen, X., Rumpagaporn, P., Seetharaman, K., & Hamaker, B. R. (2016). Small differences in amylopectin fine structure may explain large functional differences of starch. *Carbohydrate Polymers, 140*, 113–121.

Blazek, J., & Gilbert, E. P. (2011). Application of small-angle X-ray and neutron scattering techniques to the characterisation of starch structure: A review. *Carbohydrate Polymers, 85*, 281–293.

Cheetham, N. W. H., & Tao, L. (1998). Variation in crystalline type with amylose content in maize starch granules: An X-ray powder diffraction study. *Carbohydrate Polymers, 36*, 277–284.

Chung, H.-J., Liu, Q., Lee, L., & Wei, D. (2011). Relationship between the structure, physicochemical properties and in vitro digestibility of rice starches with different amylose contents. *Food Hydrocolloids, 25*, 968–975.

Ewoldt, R., Hosoi, A., & McKinley, G. (2008). New measures for characterizing nonlinear viscoelasticity in large amplitude oscillatory shear. *Journal of Rheology, 52*.

Han, X. Z., & Hamaker, B. R. (2001). Amylopectin fine structure and Rice starch paste breakdown. *Journal of Cereal Science, 34*, 279–284.

Hanashiro, I., Abe, J. I., & Hizukuri, S. (1996). A periodic distribution of the chain length of amylopectin as revealed by high-performance anion-exchange chromatography. *Carbohydrate Research, 283*, 151–159.

Hizukuri, S., Takeda, Y., & Juliano, O. B. (1995). Structural changes of non-waxy starch during development of rice grains. In *Progress in plant polymeric carbohydrates research proceeding of international symposium of plant polymeric carbohydrates* (pp. 38–41).

Hyun, K., Wilhelm, M., Klein, C. O., Cho, K. S., Nam, J. G., Ahn, K. H., & McKinley, G. H. (2011). A review of nonlinear oscillatory shear tests: Analysis and application of large amplitude oscillatory shear (LAOS). *Progress in Polymer Science, 36*, 1697–1753.

Jane, J. L., & Chen, J. F. (1992). Effect of amylose molecular size and amylopectin branch chain length on paste properties of starch. *Cereal Chemistry, 69*, 60–65.

Juliano, B. O., & Tuano, A. P. P. (2019). 2 - Gross structure and composition of the rice grain. In J. Bao (Ed.), *Rice* (4th ed., pp. 31–53). AACC International Press.

Kong, X., Chen, Y., Zhu, P., Sui, Z., Corke, H., & Bao, J. (2015). Relationships among genetic, structural, and functional properties of Rice starch. *Journal of Agriculture and Food Chemistry, 63*, 6241–6248.

Kong, X., Kasapis, S., Bertoft, E., & Corke, H. (2010). Rheological properties of starches from grain amaranth and their relationship to starch structure. *Starch - Stärke, 62*, 302–308.

Koroteeva, D. A., Kiseleva, V. I., Sriroth, K., Piyachomkwan, K., Bertoft, E., Yuryev, P. V., & Yuryev, V. P. (2007). Structural and thermodynamic properties of rice starches with different genetic background: Part 1. Differentiation of amylopectin and amylose defects. *International Journal of Biological Macromolecules, 41*, 391–403.

Korus, J., Witczak, M., Juszczak, L., & Ziobro, R. (2008). Grass pea (Lathyrus sativus L.) starch as an alternative for cereal starches: Rheological properties and retrogradation susceptibility. *Journal of Food Engineering, 88*, 528–534.

Kozlov, S. S., Krivandin, A. V., Shatalova, O. V., Noda, T., Bertoft, E., Fornal, J., & Yuryev, V. P. (2007). Structure of starches extracted from near-isogenic wheat lines. *Journal of Thermal Analysis and Calorimetry, 87*, 575–584.

Li, L., Blanco, M., & Jane, J. L. (2007). Physicochemical properties of endosperm and pericarp starches during maize development. *Carbohydrate Polymers, 67*, 630–639.

Li, Q. F., Zhang, G. Y., Dong, Z. W., Yu, H. X., Gu, M. H., Sun, S. S., & Liu, Q. Q. (2009). Characterization of expression of the OsPUL gene encoding a pullulanase-type debranching enzyme during seed development and germination in rice. *Plant Physiology and Biochemistry, 47*(5), 351–358. https://doi.org/10.1016/j.plaphy.2009.02.001

Li, R., Zheng, W., Jiang, M., & Zhang, H. (2021). A review of starch biosynthesis in cereal crops and its potential breeding applications in rice (Oryza sativa L.). *PeerJ, 9*, Article e12678.

Li, Z., Kong, X., Zhou, X., Zhong, K., Zhou, S., & Liu, X. (2016). Characterization of multi-scale structure and thermal properties of indica rice starch with different amylose contents. *RSC Advances, 6*, 107491–107497.

Lii, C., Tsai, M., & Tseng, K. H. (1996). Effect of amylose content on the rheological property of rice starch. *Cereal Chemistry, 73*, 415–420.

Liu, Z., Chen, L., Bie, P., Xie, F., & Zheng, B. (2021). An insight into the structural evolution of waxy maize starch chains during growth based on nonlinear rheology. *Food Hydrocolloids, 116*, Article 106655.

Lu, S., Chen, L. N., & Lii, C. Y. (1997). Correlations between the fine structure, physicochemical properties, and retrogradation of Amylopectins from Taiwan Rice varieties. *Cereal Chemistry, 74*, 34–39.

Oko, A., Kumar, A., Lal, M., & Sharma, S. (2018). Determination of amylose content and expression analysis of the granular-bound starch synthase I (GBSS1) gene in rice grains. *Nigerian Journal of Biotechnology, 34*, 71.

Ong, M. H., & Blanshard, J. M. V. (1995). Texture determinants in cooked, parboiled rice. I: Rice starch amylose and the fine stucture of amylopectin. *Journal of Cereal Science, 21*, 251–260.

Pantoa, T., Baricevic-Jones, I., Suwannaporn, P., Kadowaki, M., Kubota, M., Roytrakul, S., & Mills, E. N. C. (2020). Young rice protein as a new source of low allergenic plant-base protein. *Journal of Cereal Science, 93*, Article 102970.

Park, I., Kim, S. H., Chung, I. M., & Shoemaker, C. F. (2013). Effect of amylopectin long chains on measured amylose content and their correlation with pasting properties. *Starch - Stärke, 65*, 227–235.

Pitiphunpong, S., & Suwannaporn, P. (2009). Physicochemical properties of KDML 105 rice cultivar from different cultivated locations in Thailand. *Journal of the Science of Food and Agriculture, 89*, 2186–2190.

Precha-Atsawanan, S., Uttapap, D., & Sagis, L. M. C. (2018). Linear and nonlinear rheological behavior of native and debranched waxy rice starch gels. *Food Hydrocolloids, 85*, 1–9.

Ranathunga, R. A. A., & Suwannaporn, P. (2022). Young cereal grains as a new source of healthy and hypoallergenic foods: A review. *Journal of Food Science & Technology, 59*, 3336–3348.

Singh, H., Lin, J. H., Huang, W. H., & Chang, Y. H. (2012). Influence of amylopectin structure on rheological and retrogradation properties of waxy rice starches. *Journal of Cereal Science, 56*, 367–373.

Wu, A. C., Morell, M. K., & Gilbert, R. G. (2013). A parameterized model of amylopectin synthesis provides key insights into the synthesis of granular starch. *PLoS One, 8*, Article e65768.

Yoo, S. H., & Jane, J. L. (2002). Molecular weights and gyration radii of amylopectins determined by high-performance size-exclusion chromatography equipped with multi-angle laser-light scattering and refractive index detectors. *Carbohydrate Polymers, 49*, 307–314.

Zhang, C., Ma, M., Xu, Y., Xu, Z., Sui, Z., & Corke, H. (2021). Octenyl succinic anhydride modification alters blending effects of waxy potato and waxy rice starches. *International Journal of Biological Macromolecules, 190*, 1–10.

Zhang, C., Xu, Z., Liu, X., Ma, M., Khalid, S., Bordiga, M., & Corke, H. (2023). Removing starch granule-associated surface lipids affects structure of heat-moisture treated hull-less barley starch. *Carbohydrate Polymers, 303*, Article 120477.

Zhang, Z., Li, E., Fan, X., Yang, C., Ma, H., & Gilbert, R. G. (2020). The effects of the chain-length distributions of starch molecules on rheological and thermal properties of wheat flour paste. *Food Hydrocolloids, 101*, Article 105563.

Zhong, Y., Li, Z., Qu, J., Bertoft, E., Li, M., Zhu, F., & Liu, X. (2021). Relationship between molecular structure and lamellar and crystalline structure of rice starch. *Carbohydrate Polymers, 258*, Article 117616.